Microfluidic Directed Formation of Liposomes of Controlled Size

Andreas Jahn,[†] Wyatt N. Vreeland,*[,‡] Don L. DeVoe,[§] Laurie E. Locascio,[‡] and Michael Gaitan[†]

Semiconductor Electronics Division and Analytical Chemistry Division, National Institute of Standards and Technology, Gaithersburg, Maryland 20899, and University of Maryland, Mechanical Engineering, College Park, Maryland 20742

Received January 8, 2007. In Final Form: February 28, 2007

A new method to tailor liposome size and size distribution in a microfluidic format is presented. Liposomes are spherical structures formed from lipid bilayers that are from tens of nanometers to several micrometers in diameter. Liposome size and size distribution are tailored for a particular application and are inherently important for in vivo applications such as drug delivery and transfection across nuclear membranes in gene therapy. Traditional laboratory methods for liposome preparation require postprocessing steps, such as sonication or membrane extrusion, to yield formulations of appropriate size. Here we describe a method to engineer liposomes of a particular size and size distribution by changing the flow conditions in a microfluidic channel, obviating the need for postprocessing. A stream of lipids dissolved in alcohol is hydrodynamically focused between two sheathed aqueous streams in a microfluidic channel. The laminar flow in the microchannel enables controlled diffusive mixing at the two liquid interfaces where the lipids self-assemble into vesicles. The liposomes formed by this self-assembly process are characterized using asymmetric flow field-flow fractionation combined with quasi-elastic light scattering and multiangle laser-light scattering. We observe that the vesicle size and size distribution are tunable over a mean diameter from 50 to 150 nm by adjusting the ratio of the alcohol-to-aqueous volumetric flow rate. We also observe that liposome formation depends more strongly on the focused alcohol stream width and its diffusive mixing with the aqueous stream than on the sheer forces at the solvent−buffer interface.

Introduction

Liposomes have attracted great interest since their discovery in 1965[1] for a wide range of biological, pharmaceutical, and industrial applications.[1−4] It is the ability to encapsulate and thereby segregate aqueous components that leads to a variety of applications of liposomes including their use in biological systems as quantized reagent packets for the delivery of genes[5,6] and deoxyribonucleic acid (DNA) vectors, drugs or other therapeutic agents,[7−16] encapsulants of contrast agents for enhanced magnet resonance imaging (MRI) with reduced tissue interaction,[17−20] model systems for the study of biological membranes, encapsulation of cells and proteins,[21] and protective coatings for enzymes entrapped in silica sol−gel biocomposites.[22] Liposome formulations are commonly prepared by the bulk hydration of lipids in aqueous buffer to yield large, polydisperse, multilamellar liposomes. Other traditional liposome preparation methods (e.g., freeze−thaw cycling,[23] film hydration,[24] reversed phase evaporation,[25,26] normal phase integration,[24] detergent depletion,[27] and pH adjustment[24]) are also conducted through mixing of bulk phases, often leading to heterogeneous and uncontrolled chemical and/or mechanical conditions during liposome formation, hence producing liposomes that are often polydisperse in size and lamellarity. Most methods to formulate liposomes require

* To whom correspondence should be addressed. E-mail: wyatt.vreeland@nist.gov.

[†] Semiconductor Electronics Division, NIST.

[‡] Analytical Chemistry Division, NIST.

[§] University of Maryland.

(1) Bangham, A. D.; Standish, M. M.; Watkins, J. C. *J. Mol. Biol.* **1965**, *13* (1), 238−252.

(2) Gregoriadis, G. *Immunol. Today* **1990**, *11* (3), 89−97.

(3) Alving, C. R. *J. Immunol. Methods* **1991**, *140* (1), 1−13.

(4) Gregoriadis, G. *N. Engl. J. Med.* **1976**, *295* (13), 704−710.

(5) Kikuchi, H.; Suzuki, N.; Ebihara, K.; Morita, H.; Ishii, Y.; Kikuchi, A.; Sugaya, S.; Serikawa, T.; Tanaka, K. *J. Controlled Release* **1999**, *62* (1−2), 269−277.

(6) Templeton, N. S.; Lasic, D. D.; Frederik, P. M.; Strey, H. H.; Roberts, D. D.; Pavlakis, G. N. *Nat. Biotechnol.* **1997**, *15* (7) 647−652.

(7) Ramachandran, S.; Quist, A. P.; Kumar, S.; Lal, R. *Langmuir* **2006**, *22* (19), 8156−8162.

(8) Abraham, S. A.; Waterhouse, D. N.; Mayer, L. D.; Cullis, P. R.; Madden, T. D.; Bally, M. B. The liposomal formulation of doxorubicin. In *Liposomes, Part E*; Düzgünes, N., Ed.; Methods in Enzymology; Elsevier: San Diego, CA, 2005; Vol. 391, pp 71−97.

(9) Schmid, M. H.; Korting, H. C. *Crit. Rev. Ther. Drug Carrier Syst.* **1994**, *11* (2−3), 97−118.

(10) Gulsen, D.; Li, C. C.; Chauhan, A. *Curr. Eye Res.* **2005**, *30* (12), 1071−1080.

(11) Andresen, T. L.; Jensen, S. S.; Jorgensen, K. *Prog. Lipid Res.* **2005**, *44* (1), 68−97.

(12) Crosasso, P.; Ceruti, M.; Brusa, P.; Arpicco, S.; Dosio, F.; Cattel, L. *J. Controlled Release* **2000**, *63* (1−2), 19−30.

(13) Mayer, L. D.; Krishna, R.; Webb, M.; Bally, M. *J. Liposome Res.* **2000**, *10* (2−3), 99−115.

(14) Mamot, C.; Drummond, D. C.; Hong, K.; Kirpotin, D. B.; Park, J. W. *Drug Resist. Updates* **2003**, *6* (5), 271−279.

(15) Sadava, D.; Coleman, A.; Kane, S. F. *J. Liposome Res.* **2002**, *12* (4), 301−309.

(16) Pavelic, Z.; Skalko-Basnet, N.; Filipovic-Grcic, J.; Martinac, A.; Jalsenjak, I. *J. Controlled Release* **2005**, *106* (1−2), 34−43.

(17) Martina, M. S.; Fortin, J. P.; Menager, C.; Clement, O.; Barratt, G.; Grabielle-Madelmont, C.; Gazeau, F.; Cabuil, V.; Lesieur, S. *J. Am. Chem. Soc.* **2005**, *127* (30), 10676−10685.

(18) Ayyagari, A. L.; Zhang, X. D.; Ghaghada, K. B.; Annapragada, A.; Hu, X. P.; Bellamkonda, R. V. *Magn. Reson. Med.* **2006**, *55* (5), 1023−1029.

(19) Mulder, W. J. M.; Strijkers, G. J.; van Tilborg, G. A. F.; Griffioen, A. W.; Nicolay, K. *Nmr Biomed.* **2006**, *19*, (1), 142−164.

(20) Saito, R.; Krauze, M. T.; Bringas, J. R.; Noble, C.; McKnight, T. R.; Jackson, P.; Wendland, M. F.; Mamot, C.; Drummond, D. C.; Kirpotin, D. B.; Hong, K. L.; Berger, M. S.; Park, J. W.; Bankiewicz, K. S. *Exp. Neurol.* **2005**, *196* (2), 381−389.

(21) Tan, Y. C.; Hettiarachchi, K.; Siu, M.; Pan, Y. P. *J. Am. Chem. Soc.* **2006**, *128* (17), 5656−5658.

(22) Li, Y.; Yip, W. T. *J. Am. Chem. Soc.* **2005**, *127* (37), 12756−12757.

(23) Traikia, M.; Warschawski, D. E.; Recouvreur, M.; Cartaud, J.; Devaux, P. F. *Eur. Biophys. J. Biophys. Lett.* **2000**, *29* (3), 184−195.

(24) Gregoriadis, G., *Liposome technology - v.3. Targeted drug delivery and biological interaction*; CRC Press, Inc.: Boca Raton, FL, 1984; Vol. 3.

(25) Szoka, F.; Papahadjopoulos, D. *Proc. Natl. Acad. Sci. U.S.A.* **1978**, *75* (9), 4194−4198.

(26) Pidgeon, C.; McNeely, S.; Schmidt, T.; Johnson, J. E. *Biochemistry* **1987**, *26*, (1), 17−29.

(27) Fischer, T. H.; Lasic, D. D. *Mol. Cryst. Liq. Cryst.* **1984**, *102*, (5), 141−153.

10.1021/la070051a CCC: $37.00
Published on Web 04/24/2007 PAGE EST: 4.6

additional postprocessing steps, such as solvent removal,[21] membrane extrusion,[28] or sonication,[29] to yield the desired homogeneous liposome populations of controlled size. In the two latter postprocessing techniques, the initially multilamellar vesicles are torn apart into small bilayered fragments or flakes, which upon fusion self-close into the desired small unilamellar vesicles. Liposome size and size distribution are important variables for in vivo applications, where size ultimately determines drug dosage, targeting, and rate of clearance from the body.[30] Liposomes can encapsulate hydrophilic substances inside their aqueous core and lipophilic substance inside the volume of the lipid bilayer. In drug delivery application, where liposomes serve as transport vehicles, it is important to employ liposomes of small size and mondisperse size distribution. The size of liposomes, besides other factors (i.e., coating), influences the detection and clearance of liposomes by the renal system. Generally, larger liposomes are cleared more rapidly than smaller ones. Recognition of the liposomes by the complement system is assumed to be proportional to the diameter of the liposomes. Smaller liposomes have a larger curvature which inversely affects the number of recognition sites and in turn reduces the clearance by the complement system.[31] Liposomes produced with hydrodynamic focusing have diameters that can be controlled from 50 to 150 nm and are therefore of interest as vehicles for drug delivery applications because of its lowered clearance rate. Liposomes typically have a finite lifetime before they begin to "leak" their internal components, which limits the potential applications of liposome-encapsulated therapeutic agents. Methods that control liposome size during formation without the need for additional steps would simplify their preparation and allow for preparation of liposomes at the point of application, thereby potentially increasing their breadth of implementation. This method is not to be confused with droplet formation processes in microfluidic systems conducted by other groups[32−34] where droplet formation is based on interfacial tension between two immiscible fluids. We apply a diffusive mechanism in a miscible two-phase system for the formation of monodisperse vesicles in which fully solvated lipids self-assemble into liposomes as the two phases (alcohol and water) interdiffuse. We first reported microfluidic liposome formation in an earlier communication.[35] In this work we report significant modifications to the system that have greatly improved our ability to control liposome size and elucidate the mechanism that controls liposome size and homogeneity. Deep channels of higher aspect ratio with rectangular cross-sectional area result in a more homogeneous velocity profile across the channel height and reduce the impact of surface effects at the bottom and top of the channel compared to previously reported shallow trapezoidal channels. Additional adjustments of the respective channel widths which alters the hydraulic resistance allows for improved focusing at reduced sample consumption. This liposome formation occurs in a continuous-flow planar microfluidic network and results in precise control of size over the diameter range of 50−150 nm through the manipulation of liquid flow rates. We show that reducing the length scale of liquid mixing to a few micrometers and less facilitates reproducible diffusive mixing and concentration gradients, thereby controlling liposome size and size distribution. We believe that the degree with which microfluidics can control liposome self-assembly could potentially open applications for on-demand liposome-mediated delivery of point-of-care personalized therapeutics.

Experimental Section[36]

Device Fabrication. Microfluidic channels were fabricated in a silicon wafer (76.2 mm (3 in.) diameter, 305−355 μm thick, Nova Electronics Materials, Inc., Carrollton, TX) with deep reactive ion etching (DRIE) using the Bosch process and sealed by anodic bonding to a borosilicate glass (BSG) wafer (75 mm diameter, 0.1 mm thick, Corning Pyrex 7740). The resulting channels had a rectangular cross section with a depth of 100 μm and a width of either 42 or 64 μm. Rectangular fluidic access through-holes of the same width as the microfluidic channel were etched from the backside of the wafer by DRIE at each channel terminus prior to bonding of the BSG wafer to the silicon wafer. The wafers were then oxidized to form a homogeneous glass surface and then anodically bonded (400 °C for 60 min with a ramp rate of 25 °C/min and a bonding voltage of 800 V) to a BSG wafer to seal the channels. Polyetheretherketone (PEEK) tubing was attached to the fluidic access points using commercially available Nanoports (F-124S, Upchurch Scientific, Oak Harbor, WA). The Nanoports were bonded to the backside of the silicon wafer according to manufacturer's directions. PEEK capillary tubes (Upchurch Scientific, Oak Harbor, WA) with an inner diameter of 254 μm (0.01 in.) connected the Nanoports to a syringe. A 0.02 μm filter (Anatop, Whatman, NJ) was placed on the syringes to ensure all fluids introduced to the microchannel network were dust-free to prevent clogging of the channels. Fluidic reagents were introduced to the microfluidic network from glass gastight syringes (Hamilton, Reno, NV) by syringe pumps (model PHD 2000, Harvard Apparatus Inc., Holliston, MA).

Preparation of the Lipid Mixture and Hydration Buffer. Dimyristoylphosphatidylcholine (DMPC), cholesterol (both Avanti Polar Lipids Inc., Alabaster, AL), and dihexadecyl phosphate (DCP) (Sigma-Aldrich) in a molar ratio of 5:4:1 were dissolved in dry chloroform (Mallinckrodt Baker Inc., Phillipsburg, NJ). The chloroform solvent was evaporated under a stream of nitrogen at room temperature to form a dry lipid film on the bottom of a scintillation vial. The scintillation vial was then placed into a vacuum desiccator for at least 24 h to ensure complete solvent removal. The dried lipid mixture was redissolved in dry isopropyl alcohol at a 5 mmol/L concentration of total lipid. Phosphate buffered saline (PBS) solution (10 mmol/L phosphate, 2.7 mmol/L potassium chloride, 138 mmol/L sodium chloride, pH 7.4, 3 mmol/L sodium azide) was used as a hydration buffer.

Liposome Preparation. Unilamellar liposomes were prepared by injecting a lipid mixture dissolved in isopropyl alcohol (IPA) into the center channel of the microfluidic network shown in Figure 1. PBS is injected into two oblique side channels intersecting with the center channel. The flow rate ratio (FRR), defined as buffer volumetric flow rate (VFR), Q_B, to IPA VFR, Q_S, was varied from 10 to 60. Liposome formation at different shear forces was investigated by changing the flow rates of the buffer streams from 15 to 90 μL/min and the alcohol stream from 1 to 6 μL/min, maintaining a constant FRR of 30.

Microscopic Imaging. The hydrodynamically focused sheathed flow in the microfluidic channel was imaged with a confocal laser scanning microscope (LSM 510 Meta, Carl Zeiss, Thornwood, NY)

(28) Batzri, S.; Korn, E. D. *Biochim. Biophys. Acta* **1973**, *298* (4), 1015−1019.
(29) Maulucci, G.; De Spirito, M.; Arcovito, G.; Boffi, F.; Castellano, A. C.; Briganti, G. *Biophys. J.* **2005**, *88*, (5), 3545−3550.
(30) Litzinger, D. C.; Buiting, A. M. J.; Vanrooijen, N.; Huang, L. *Biochim. Biophys. Acta* **1994**, *1190* (1), 99−107.
(31) Ishida, T.; Harashima, H.; Kiwada, H. *Biosci. Rep.* **2002**, *22* (2), 197−224.
(32) Thorsen, T.; Roberts, R. W.; Arnold, F. H.; Quake, S. R. *Phys. Rev. Lett.* **2001**, *86* (18), 4163−4166.
(33) Anna, S. L.; Bontoux, N.; Stone, H. A. *Appl. Phys. Lett.* **2003**, *82* (3), 364−366.
(34) Link, D. R.; Anna, S. L.; Weitz, D. A.; Stone, H. A. *Phys. Rev. Lett.* **2004**, *92* (5), 054503(4).
(35) Jahn, A.; Vreeland, W. N.; Gaitan, M.; Locascio, L. E. *J. Am. Chem. Soc.* **2004**, *126* (9), 2674−2675.

(36) Certain commercial materials and equipment are identified in order to specify adequately experimental procedures. In no case does such identification imply recommendation or endorsement by the National Institute of Standards and Technology, nor does it imply that the items identified are necessarily the best available for the purpose.

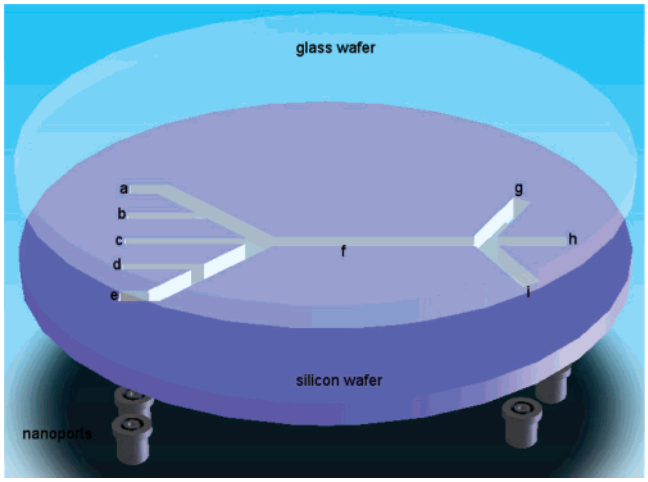

Figure 1. Schematic of the microfluidic device. Exploded view showing the fluid ports attached to the backside of the silicon wafer, the channel network etched into silicon with five inlet channels (a−e) on the left and three outlet channels (g−i) on the right, and the sealing with a glass wafer via anodic bonding.

with a 30 mW HeNe laser (excitation, 543 nm; power output, 18%; objective LD-Achroplan, 20×/0.4; detector gain, 468; amplifier gain, 1.00 V; amplifier offset, 0.1 V; filter, LP 560; beamsplitter, MBS HFT 488/543; 12-bit image resolution; 1.6 μs pixel time; 94 μm pinhole). Image processing software was provided by the vendor (Carl Zeiss). Alcohol concentration was determined by measuring the quantum efficiency of sulforhodamine B as it varies with alcohol concentration.

Light Scattering and Asymmetric Flow Field-Flow Fractionation (AF^4) Procedure. High-resolution size-based separation of the liposome population was carried out using AF^4 with multiangle laser light scattering (MALLS) and quasi-elastic light scattering (QELS) detection and characterization (model DAWN EOS and QELS, Wyatt Technology, Santa Barbara, CA). A vendor-supplied spacer (250 μm thickness) was used to define the flow channel thickness with a 10 kg/mol MWCO regenerated cellulose membrane for the cross-flow partition (Millipore, Bedford, MA). The carrier liquid used in the separation was PBS. The flow was controlled with vendor-supplied software (Eclipse 2, Wyatt Technology, Santa Barbara, CA). A sample volume of 100 μL was injected at a flow rate of 0.2 μL/min while focusing at 3 mL/min for 4 min. The injection step was followed by a second focusing step at 3 mL/min for 3 min. The crossflow was ramped linearly from 3 to 0 mL/min over 60 min while eluting the separated particles at 0.8 mL/min. The radii of the eluted fractions were monitored using the MALLS and QELS detectors with data processing using software supplied by the vendor (ASTRA, Wyatt Technology, Santa Barbara, CA). Static light scattering intensity was measured at 15 angles simultaneously, and liposome concentrations were determined by applying the refractive index increment.[37] The sample was measured at 1 s intervals for the MALLS and 5 s intervals for the QELS. The autocorrelation function of the QELS was fitted to a single-mode exponential decay model to determine the hydrodynamic radius. A coated sphere model (i.e., a spherical structure with two radial regions of differing refractive index) showing good fit with the MALLS data (data not shown) was applied for size analysis of the geometric radius of the fractionated samples.

Results and Discussion

Hydrodynamic Focusing. Hydrodynamic focusing in a microfluidic device allows for fast and controlled mixing of miscible liquids with the benefit of reduced sample consumption. In the microfluidic device presented in Figure 1, four aqueous buffer streams (channels a, b, d, and e in Figure 1) hydrodynamically focus a lipid tincture entering through the center channel (channel c in Figure 1) at the cross junction. Hydrodynamic focusing reduces the center channel stream width and consequently the diffusion length for liquids to mix. The sample stream (channel c, Figure 1) is focused into a thin sheet whose width is inversely proportional to the ratio of Q_B to Q_S and proportional to Q_S. Simple mass flow balance within the microchannel can provide a theoretical model to estimate the absolute minimum continuum width of the focused sample stream

$$Q_S = v_f w_{fs} h = v_c D_c h \quad (1)$$

so that

$$w_{fs} = \left(\frac{D_f}{1 + \frac{Q_B}{Q_S}} \right) \quad (2)$$

where w_{fs} is the stream width of the focused sample stream in channel f (see Figure 1), Q_S and Q_B are lipid mixture and buffer volumetric flow rate, v_c and v_f are the mean flow velocities of channels c and f, D_c and D_f are the widths of channels c and f, respectively, and h is the channel height which is constant for the entire microchannel network. The focused stream width, w_{fs}, is computed under the simplifying assumptions that (1) all liquids entering the channels have the same density, (2) all liquids have a parabolic flow profile across the width of the channel, and (3) diffusive mixing does not occur. Equation 2 shows that w_{fs} depends only on the microchannel geometry and the FRR of Q_B to Q_S. Equation 2 provides an estimate of the focused sample stream width within the first 100 μm to 300 μm of the entrance of channel f of the hydrodynamically focused stream at low FRR. Although diffusion is neglected in eq 2, it is suitable to estimate the width of the focused stream in the entrance region of channel f. The stream width estimated from eq 2 agrees with the stream width measured in Figure 2 at flow rate ratios 5 and 10. At higher FRR the distance IPA diffuses is substantial compared to the estimated stream width, and diffusion must be considered for accurate stream width estimates. Figure 2 shows confocal microscope images of the IPA concentration across and along the center channel as a function of increasing FRRs from 5 on the left to 35 on the right in increments of 5. Figure 3 depicts the alcohol concentration along the centerline for the last 100 μm in channel c and the first 300 μm in channel f. The sharp drop in alcohol concentration between about 80 and 170 μm is due to the decreasing stream width of the IPA stream as

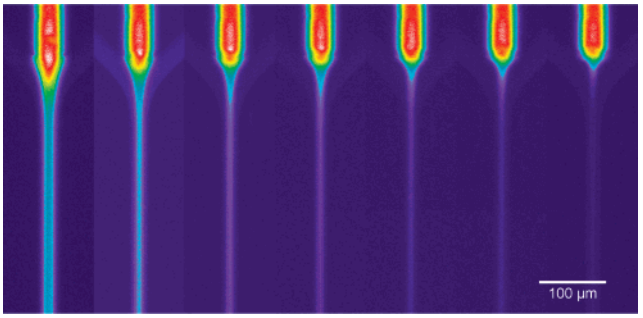

Figure 2. False color confocal microscope images showing hydrodynamic focusing of an IPA stream by two adjacent aqueous buffer streams (not visible). The focused IPA stream containing sulforhodamine B for visualizing purposes enters from the top. Shown are 7 different flow rate ratios (FRRs), increasing from 5 to 35 in increments of 5 from left to right at a total constant volumetric flow rate (VFR) of 100 μL/min.

(37) Wyatt, P. J.; Weida, M. J. Method and Apparatus for Determining Absolute Number Densities of Particles in Suspension. U.S. Patent 6,774,994 B1, Aug 10, 2004.

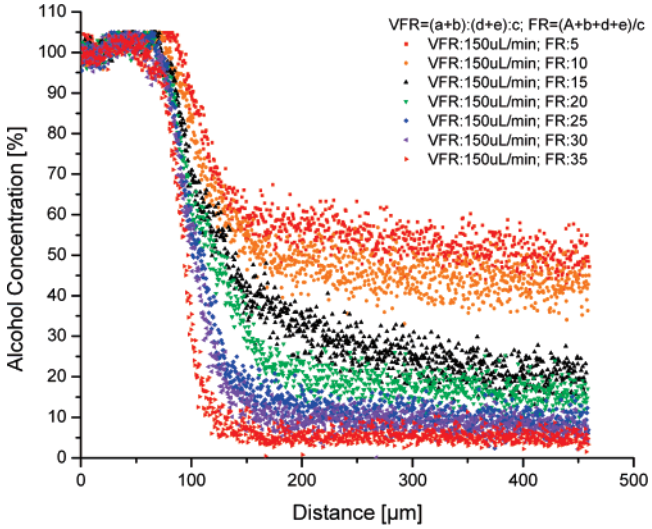

Figure 3. Isopropyl alcohol (IPA) concentration along the center of the center-channel as a function of distance. As the FRR between buffer and sample stream was increased 7-fold from 5 to 35 at a constant total volumetric flow rate, tVFR, of 150 μL/min, the IPA concentration decreases stronger along the center channel. The IPA concentration was determined with a confocal laser scanning microscope by measuring the quantum efficiency of sulforhodamine B dissolved in IPA.

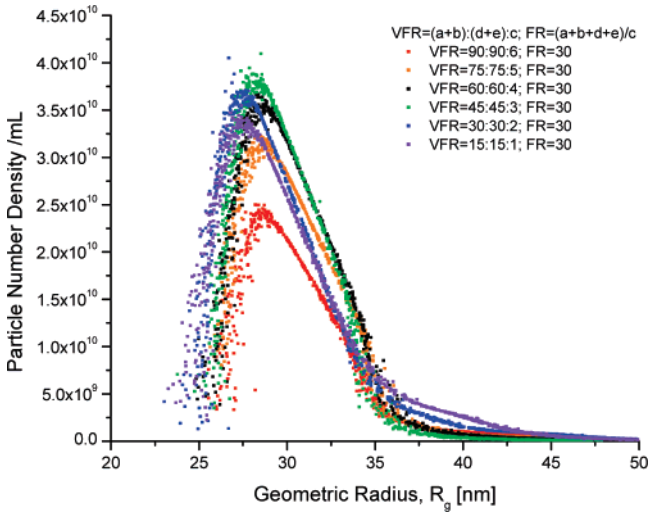

Figure 4. Data shown illustrate liposome size and size distribution at a constant FRR and different VFRs. As the VFR increases 6-fold, the liposome size and size distribution remain nearly constant, indicating that the magnitude of shear stresses during liposome self-assembly does not substantially influence liposome size or size distribution.

it is hydrodynamically focused by two adjacent buffer streams. As the FRR increases, the alcohol stream width decreases. A smaller alcohol stream width results in a shorter diffusion length, and therefore the IPA concentration decreases more sharply along a given channel length. The hydrodynamic focusing process is completed after about 150 μm when the stream enters channel f and then the concentration of IPA decreases due to diffusion. Laminar flow conditions in the channel allow for mixing that is based entirely on molecular diffusion in a direction normal to liquid flow streamlines. At a critical alcohol-to-water ratio the lipid monomers in the alcohol stream become insoluble and spontaneously self-assemble into closed spherical structures concomitantly sequestering the surrounding fluid. A smaller w_{fs} results in reduced diffusion lengths for mixing of the alcohol center stream and aqueous side stream, thereby reducing the

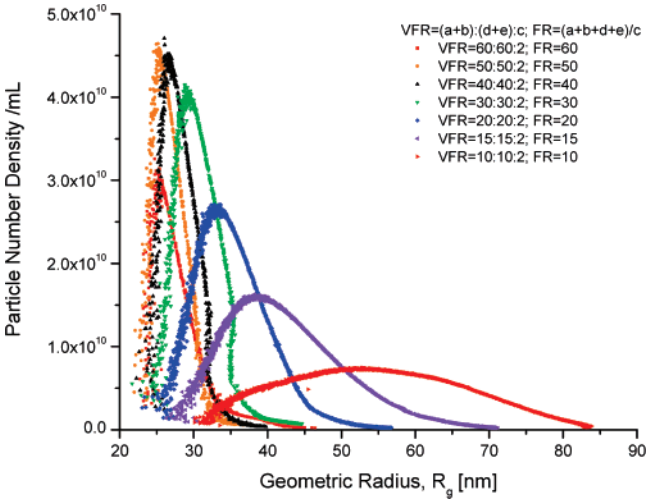

Figure 5. Data shown illustrate liposome size and size distribution at different FRRs. As the FRR increases 6-fold, the liposome size decreases in diameter from approximately 120 to 50 nm and the size distribution decreases from $\pm$50 nm to $\pm$10 nm ($\approx 3\sigma$).

distance in the center channel distal from the mixing intersection to reach the critical alcohol concentration where lipids spontaneously self-assemble into spherical vesicles. The effects of total VFR and FRR between sheath and sample flow on liposome formation were investigated using MALLS and QELS combined with AF4.

Influence of Total Volumetric Flow Rate and Shear Force on Liposome Formation. Figure 4 presents measurements of liposome number density versus liposome size and size distribution for six different total VFRs ranging from 30 to 180 μL/min at a constant FRR of 30. At a constant FRR, the width of the focused lipid/alcohol stream remains constant because the liquid is incompressible, and therefore the stream width, and thus the dilution rate, does not depend on the magnitude of the inlet and side channel VFRs but on the ratio of inlet and side channel VFRs. By maintaining a constant FRR and increasing the flow rates, the stream width and dilution rate are held constant; however, the shear forces at the interface of the two fluids increase.

As the VFR is increased 6-fold from 30 to 180 μL/min, the eluted liposomes were of approximately the same size and size distribution with a mean geometric radius of 29 nm and a distribution of $\pm$4 nm ($\approx 3\sigma$) as is shown in Figure 4. This indicates that the absolute magnitude of the shear forces between the parallel layered streams have no significant impact on liposome size or size distribution. The increased noise in the data at a geometric radius less than 27 nm is due to lower concentrations and smaller sizes of particles, yielding a lower excess Rayleigh ratio.

Influence of Flow Rate Ratio on Liposome Formation. Figure 5 and Figure 6 show liposome size and size distribution at different FRRs. It is observed that as the FRR decreases, the mean liposome size increases and the size distribution becomes more disperse. One possible mechanism to explain this phenomenon is as follows: assuming that the lipids are homogeneously distributed in the alcohol stream, when the alcohol stream first comes into contact with the aqueous streams, the lipids at that interface will quickly reach the critical alcohol concentration and self-assemble into liposomes. The resulting liposomes have a markedly decreased diffusion coefficient and will convect along the stream lines of the fluid flow. It is then possible that as the alcohol continues to diffuse, the alcohol concentration will increase in a direction normal to the streamlines. If there is enough alcohol in the common alcohol-aqueous stream (i.e., the alcohol portion of the stream is wide enough), it will cause the local

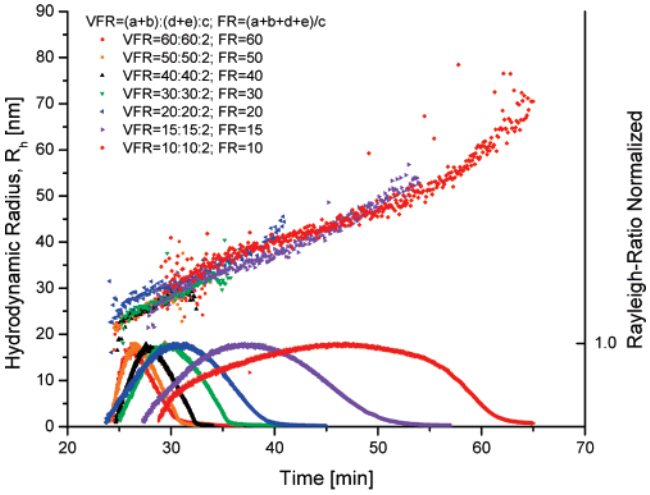

Figure 6. This graph shows QELS measurements of the hydrodynamic radius R_h of liposomes as they elute from AF^4 as a function of time at different FRRs. At low FRR the R_h of the liposomes varies between 30 and 70 nm, representing a rather broad liposome size distribution. With increasing FRR (30 and higher) the mean R_h decreases and the liposome size distribution becomes increasingly narrower with R_h varying between 22 and 27 nm. It also shows the Rayleigh scattering ratio of the liposomes which depends on liposome number and liposome size. The Rayleigh scattering in this graph provides information about the amount of liposomes as they elute over time.

alcohol concentration around the liposomes that were formed at the initial interface to increase above the critical concentration for liposome formation and the liposomes to partially disassemble. As the two streams continue to mix, the alcohol concentration near the initially formed liposomes will again decrease below the critical concentration, causing the liposome to reassemble. As the FRR decreases, the amount of alcohol introduced to the system and the alcohol stream width increase, causing the alcohol concentration to remain above the critical alcohol concentration for a longer length of the channel, and the magnitude of this phenomenon will increase. In contrast, as the FRR increases, the amount of alcohol in the system decreases, and fewer liposomes will experience alcohol concentrations high enough to induce this disassembly−reassembly phenomenon. Further increases in FRR lead to smaller changes in the stream width and the size and size distribution asymptotically approach limits which are dependent on the maximum focusing of the center stream by the four buffer streams. Experiments to verify and more fully characterize this putative mechanism for increased size and polydispersity are underway in our laboratories.

Figure 6 shows QELS measurements of the hydrodynamic radius, R_h, of liposomes at different FRRs as a function of time as the liposomes elute from the AF^4 channel. QELS, through measurement of time-dependent fluctuations of scattered light, determines the diffusion constant, D, of the particles. Typically, this is reported as R_h, which is the radius of a sphere that has the same D as the measured particles. Measurement of R_h with QELS and R_g with MALLS allows for additional compositional characterization of the liposomes with respect to lamellarity. From the data observed for R_h and R_g (data not shown), it can be concluded that the liposomes are predominantly of unilamellar configuration.

Conclusion

The creation of liposomes using microfluidic techniques has been demonstrated to produce formulations of monodisperse distributions whose size can be controlled by adjusting the fluid flow rates in the microfluidic network. Microfluidics allow for precise control of mixing via molecular diffusion with reproducible and controlled mechanical fluid forces over micrometer length scales. Decreasing the sample stream width to micrometer length scales allows for controlled and reproducible mechanical and chemical conditions across the stream width, especially compared to more traditional bulk-phase preparation techniques (i.e., test tubes and beakers). The laminar flow and precise fluidic control of the microchannel enables reproducible flow fields for the self-assembly of lipids in the sheathed flow field. Our latest measurements indicate that the formation of liposomes is mediated by the diffusion of solvent but not the difference of the mechanical shear forces between the miscible phases. The liposome self-assembly strategy described here could be implemented for point-of-care drug encapsulation; thus, liposome-mediated drug delivery could eliminate shelf life limitations of the liposome preparation.

LA070051A